AGARD-CP -331

AGARD

ADVISORY GROUP FOR AEROSPACE RESEARCH & DEVELOPMENT

7 RUE ANCELLE 92200 NEUILLY SUR SEINE FRANCE

AGARD CONFERENCE PRINT No. 331

Propagation Effects of ECM Resistant Systems in Communication and Navigation

30th Symposium
of the Electromagnetic Wave Panel
Copenhagen, Denmark, 24–28 May 1982

NORTH ATLANTIC TREATY ORGANIZATION

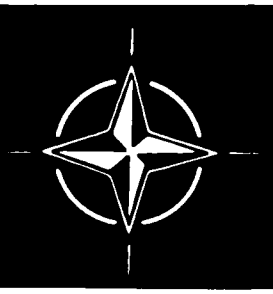

SECURITY CLASSIFICATION OF THIS PAGE (When Data Entered)

REPORT DOCUMENTATION PAGE

READ INSTRUCTIONS BEFORE COMPLETING FORM

1. REPORT NUMBER: 16638.15-GS	2. GOVT. ACCESSION NO.: AD-A116 433 N/A
3. RECIPIENT'S CATALOG NUMBER: N/A	
4. TITLE (and Subtitle): The Atmospheric Propagation Medium Between 45 and 75 GHz	5. TYPE OF REPORT & PERIOD COVERED: Reprint
	6. PERFORMING ORG. REPORT NUMBER: N/A
7. AUTHOR(s): Hans J. Liebe	8. CONTRACT OR GRANT NUMBER(s): ARO 6-82
9. PERFORMING ORGANIZATION NAME AND ADDRESS: Institute for Telecommunication Sciences, Boulder, CO 80303	10. PROGRAM ELEMENT, PROJECT, TASK AREA & WORK UNIT NUMBERS: N/A
11. CONTROLLING OFFICE NAME AND ADDRESS: U. S. Army Research Office, P. O. Box 12211, Research Triangle Park, NC 27709	12. REPORT DATE: 1982
	13. NUMBER OF PAGES: 13
14. MONITORING AGENCY NAME & ADDRESS (if different from Controlling Office)	15. SECURITY CLASS. (of this report): Unclassified
	15a. DECLASSIFICATION/DOWNGRADING SCHEDULE

16. DISTRIBUTION STATEMENT (of this Report)

Submitted for announcement only.

17. DISTRIBUTION STATEMENT (of the abstract entered in Block 20, if different from Report)

18. SUPPLEMENTARY NOTES

19. KEY WORDS (Continue on reverse side if necessary and identify by block number)

20. ABSTRACT (Continue on reverse side if necessary and identify by block number)

A-21

DD FORM 1 JAN 73 1473 EDITION OF 1 NOV 65 IS OBSOLETE

Unclassified

SECURITY CLASSIFICATION OF THIS PAGE (When Data Entered)

AGARD 31st MEETING OF THE EM WAVE PROPAGATION PANEL
Denmark 24-28 May, 1982

PROPAGATION EFFECTS OF EMC-RESISTANT SYSTEMS
IN COMMUNICATION AND NAVIGATION

THE ATMOSPHERIC PROPAGATION MEDIUM BETWEEN 45 AND 75 GHz

Hans J. Liebe
Institute for Telecommunication Sciences
National Telecommunication and Information Administration
U.S. Department of Commerce
Boulder, Colorado 80303

SUMMARY

The clear atmosphere (dry air mass) represents a unique filter over the 45 to 75 GHz range with frequency-dependent absorption properties caused by the microwave spectrum of oxygen not found at any lower frequency. The basic information necessary for determining molecular line, band, and continuum absorption is contained in a transfer function model. Close to sea level, an unstructured band exists, centered at 60 GHz with a half-width of 8 GHz and a pressure-dependent intensity that is corrected for pressure-induced line overlap effects. At elevations above 12 km, the lines separate and radio channels with up to 400 MHz bandwidth can be accommodated between lines. Above 30 km, the line properties become polarization and orientation (i.e., with respect to the direction of a magnetic field) dependent due to the Zeeman effect. Each oxygen line splits proportionally with geomagnetic field strength (0.2-0.8 Gauss) into numerous sub-lines, which conform to Zeeman patterns extending over a megahertz scale around each line center.

Using this model in computer routines in conjunction with distributions of pressure, temperature, and humidity along a radio path makes it possible to predict frequency-dependent signal attenuation and delay effects of the neutral atmosphere (h=0 to 100 km). Further analysis investigates possible bandwidth limitations of the propagation medium by employing short-pulsed ($\leq$ 1 ns) test signals with carriers in the 45 to 75 GHz range. Examples are presented of specific attenuation (dB/km) and excess delay (ps/km) rates, of zenith path attenuation (dB), and of pulse distortion over a terrestrial link (50 GHz, 35 km) for Gaussian, rectangular, and BPSK modulation. Benefits from the frequency-variable atmospheric properties include a fairly well defined signal range, affording transmission security and trade-offs between range and susceptibility to detection and interference.

1. INTRODUCTION

The clear, nonturbulent atmosphere sets limits on the transmission of radio waves in the 45 to 75 GHz frequency interval. Absorption due to O_2 causes signal attenuation, changes in transit time, and increases in the background noise. Accurate knowledge of the atmospheric transfer function provides the basis for a variety of specialized applications including:

- Broadband communication with a restricted and/or frequency-dependent radio path range;
- Shielding of satellite-to-satellite links from ground interferences;
- Secure communication between high-flying aircraft and aircraft-to-satellite links;
- Remote sensing of vertical temperature profiles from satellite or ground-based observation platforms.

In the past, the accuracy of predicting atmospheric transfer properties from meteorological data was poor. ITS developed a new spectrometer which measures dispersion-pressure-profiles. These were reduced to reliable spectroscopic coefficients for the more than 30 oxygen absorption lines centered around 60 GHz [LIEBE et al., 1977]. The extensive laboratory data reduce errors in predicting attenuation rates over the range 0.1 to 20 dB/km to a few percent (1 to 3%). The standard microwave refractivity with two coefficients (dry and wet term) was expanded into a 250-coefficients-scheme computer model [LIEBE, 1981]. This paper discusses the modeling strategy and provides a series of mostly graphical outputs, which elucidate the influence that frequency, range, humidity, altitude, and geomagnetic field strength have upon transfer properties of the neutral atmosphere over the height range h=0 to 100 km.

2. ATMOSPHERIC TRANSFER PROPERTIES

2.1 Transfer Function and Specific Propagation Rates

Amplitude and phase response of a planar radio wave traveling the distance L in km and starting with the field strength E_o are described by the transfer function

$$\Gamma = (E/E_o) = \exp(\Gamma L) = \exp[j0.02096f(10^6 + N)L] \qquad (1)$$

where frequency f is in gigahertz (GHz) and Γ in km^{-1} is the propagation constant.

Germane to any propagation model is a convenient macroscopic measure of the interaction between radiation and the atmosphere. Complex refractivity N (in parts per million), expressed in terms of measurable quantities, assumes that role. For air, N consists of three components

$$N = N_o + D(f) + jN''(f) \text{ ppm} \qquad (2)$$

namely, the frequency independent refractivity N_o plus various spectra of refractive phase dispersion D(f) and absorption N"(f). Usually, the imaginary part of Eq. 2 is expressed as the specific power attenuation α and the real part determines the phase delay β (with reference to vacuum) as follows:

$$\alpha = 0.1820 f N'' \quad \text{dB/km} \tag{3}$$

and

$$\beta = 0.02096 f(N_o + D) \quad \text{radians/km} \tag{4}$$

Accordingly, the propagation constant Γ and the excess propagation delay time t are

$$\Gamma = -0.1151\alpha + j(2.096 \cdot 10^4 f + \beta) \quad 1/\text{km} \tag{5}$$

$$t = (\beta/2\pi f)\, 10^3 = 3.336(N_o + D) \quad \text{ps/km.} \tag{6}$$

2.2 Complex EHF Refractivity of Air

The frequency-independent refractivity is given by [LIEBE, 1981]

$$N_o = (2.589p + 41.6e\theta + 2.39e)\theta \quad \text{ppm} \tag{7}$$

and can be calculated in a straightforward manner. A physical state of air, which determines the absorber population in a radio path, is described by

p	dry air pressure (barometric pressure $P = p + e$), kPa (1 kPa = 10 mbar);	(8)
$\theta = 300/T$	relative inverse temperature (T in K);	
e	water vapor partial pressure, kPa; and	
w	cloud water concentration, g/m^3	

The absorption and dispersion spectra are formulated from line contributions, a continuum N_c, and a cloud water term N_w; i.e.,

$$N''(f) = \sum_i (SF'')_i + N''_c + N''_w \quad \text{ppm} \tag{9}$$

and

$$D(f) = \sum_i (SF')_i + N'_c + N'_w \quad \text{ppm} \tag{10}$$

Both expressions are discussed in detail by LIEBE [1931].

Oxygen absorption, which dominates in the 45 to 75 GHz range, is calculated from the line strength

$$S = a_1 p\theta^3 \exp[a_2(1 - \theta)] \quad \text{kHz} \tag{11}$$

and the shape factors F"(f) and F'(f).

For the line shape, we chose the VanVleck-Weisskopf function as modified by ROSENKRANZ [1975]:

$$F'' = \frac{f}{\nu_o}\left[\frac{\gamma - (\nu_o - f)\delta}{(\nu_o - f)^2 + \gamma^2} + \frac{\gamma - (\nu_o + f)\delta}{(\nu_o + f)^2 + \gamma^2}\right] \quad \text{GHz}^{-1} \tag{12}$$

A Hilbert transform of (12) yields the dispersion profile [BROWN, 1982]

$$F' = \frac{(\nu_o - f) + \gamma(\gamma + \delta f)/\nu_o}{(\nu_o - f)^2 + \gamma^2} + \frac{(\nu_o + f) + \gamma(\gamma - \delta f)/\nu_o}{(\nu_o + f)^2 + \gamma^2} - \frac{2}{\nu_o} \quad \text{GHz}^{-1} \tag{13}$$

which is slightly different from F' given by LIEBE [1981]. The line parameters are

$$\gamma = a_3(p + 1.3e)\theta^{0.9} \quad \text{GHz} \tag{14}$$

$$\delta = a_4 p\theta^{a_5} \quad 1 \tag{15}$$

where γ is the width and $|\delta| < 1$ is the overlap interference. The spectroscopic coefficients $a_{1\text{-}5}$ and the molecular line center frequencies ν_o for i = 46 O_2 lines, as well as for i = 30 H_2O lines, are tabulated by LIEBE [1981].

The continuum spectrum consists of a water vapor and a dry air absorption term,

$$N''_c = f\theta^3\{19e + 74p/[f^2 + (0.012p\theta)^2]\}10^{-6} \quad \text{ppm} \tag{16}$$

while refractive continuum phase dispersion is neglected, that is

$$N'_c = 0 \tag{17}$$

Liquid water extinction N''_w of suspended droplets (cloud, fog, haze, aerosol hydrometeors) can be derived from dielectric data of bulk water given by

$$\varepsilon' = 4.9 + (185.1 - 113/\theta)/[1 + (f\tau)^2]$$

and (18)

$$\varepsilon'' = f\tau(185.1 - 113/\theta)/[1 + (f\tau)^2]$$

where

$$\tau = 0.417\theta\ 10^{-4} \exp(7.13\theta) \quad \text{ns} \tag{19}$$

The Rayleigh absorption approximation

$$N''_w = 4.49w\ \varepsilon''/[(\varepsilon' + 2)^2 + (\varepsilon'')^2] \tag{20}$$

of Mie scattering losses is appropriate, and refractive dispersion is neglected (i.e., $N'_w = 0$).

2.3 Radio Path Transfer Function

While equations (3) and (4) describe the specific rates α and β of a homogeneous air volume element over a path increment dx, the propagation medium of an extended radio path generally is inhomogeneous. Total path attenuation A and excess delay ϕ over a length L are evaluated as follows:

$$A = \int_0^L \alpha(x)dx \quad \text{dB}$$

and (21)

$$\phi = \int_0^L \beta(x)dx \quad \text{radians}$$

Equation (21) allows us to define a radio path transfer function

$$T_L = \exp(-0.115A + j\phi) \tag{22}$$

The excess propagation delay time of the path is

$$t_L = 0.159\phi/f \quad \text{ns}. \tag{22a}$$

3. ATMOSPHERIC TRANSFER PROPERTIES FOR ALTITUDES 0 to 30 KM

The complex refractivity N (Eq. 2), as formulated in Section 2.2, is evaluated by a computer routine, which produces values of attenuation $\alpha(f)$, dispersion D(f), and refractivity N_0. The program is valid for frequencies up to 1000 GHz and for heights up to 30 km. In the troposphere (h < 10 km), only lines of H_2O and O_2 are important. The calculation of N(f, P, T, e, w) is done in a subroutine using line-by-line superposition at each frequency, the continuum (Eq. 16), and the suspended hydrometeor absorption (Eq. 20). Water vapor pressure, e(kPa), absolute humidity, v (g/m^3), or relative humidity, RH(%), can be specified.

The main program generates a frequency grid with a resolution that is tied to the line center frequencies which fall within the desired range. Two consecutive values, ν'_0 and ν''_0, are taken and the number of points between them is specified (usually 2 to 5). Also automatically added to the grid are the half-power points at $\nu_0 \pm \gamma$. Thus it is assured that attenuation maxima and dispersion peaks will be plotted. The program feeds one frequency at a time into the subroutine and receives values of α and D, which are stored temporarily in two arrays. When all numbers of the grid have been processed, the output is presented in a numerical printout and processed by a graphics routine. Examples are depicted in Figs. 1 to 3 and Table I, taking w = 0.

An overview of the full program to 1000 GHz at sea level is given in Fig. 1. Significant attenuation extends over several orders of magnitude, and above 120 GHz is caused mainly by water vapor. The low-frequency wing of the dispersion spectrum from the strong 557-GHz H_2O line makes its influence known down to about 50 GHz. The frequency range 45 to 75 GHz is dominated by oxygen absorption, as evident from Figs. 2 and 3. The change in attenuation from h=0 to 6 km is small. Above h=10 km, however, one can see a significant difference – the unstructured 60 GHz band shape transforms into a highly-structured single line response with distinct peaks and valleys. The lines narrow with increasing altitude, deepening the valleys while the line peaks stay approximately constant. This behavior is illustrated in Fig. 3 in more detail and backed by selected numerical examples in Table I. Tracing the line peaks to zero intensity over the range h=30 to 100 km introduces complications of Zeeman splitting by the weak geomagnetic field (0.3 to 0.6 Gauss), which is discussed in the following section.

Frequency-agile systems which operate within the 60 GHz band can have the capability of selecting a desired atmospheric path attenuation to limit range or afford interference protection. Fixed rates up to $\alpha \leq 10$ dB/km can be realized below h=8 km, and they drop to $\alpha \leq 1$ dB/km at h=16 km. Another property of the 60 GHz band is a frequency-dependent temperature dependence of α and β. Applying the approximations

$$\alpha(T) = \alpha(300K)\theta^x \quad \text{and} \quad \beta(T) = \beta(300K)\theta^y \tag{23}$$

to sea level air, we obtain [LIEBE and HOPPONEN, 1977] (α,β - see Table III and Fig. 2):

f	50	55	60	65	70 GHz
x	2.49	1.30	2.35	1.20	2.71
y	1.84	1.98	3.30	1.87	1.88

4. MESOSPHERIC PROPAGATION MODEL

The model calculates specific attenuation of a single line above h = 30 km. Decreasing pressure in Eq. (14) causes it to eventually approach the finite Doppler line width

$$\gamma_D = 6.20\nu_o/\sqrt{m\vartheta} \quad \text{kHz} \tag{24}$$

where m is the molecular weight (e.g., O_2, m = 32, ϑ = 1, ν_o = 60 GHz; γ_D = 65.8 kHz). An adequate approximation can be made by replacing γ with

$$\gamma_h = \sqrt{\gamma^2 + \gamma_D^2} \tag{25}$$

Zeeman splitting of isolated oxygen lines due to the influence of the earth's magnetic field strength H introduces considerable complications. Each line is identified by a quantum number K. The presence of the steady field H splits $K^{\pm}$ lines into three groups of $(2K^{\pm} \mp 1)$ sublines, thereby redistributing line attenuation over a fixed frequency range. In principle, three different Zeeman patterns, $\alpha_{1,2,3}$, are possible for any $K^{\pm}$ line. These patterns are obtained by evaluating n and ξ coefficients in π and $\sigma^{\pm}$ groups as detailed by LIEBE [1981]. Each sum of sublines determines a Zeeman pattern according to

$$\alpha_{1,2,3} = \alpha_o \sum \xi / \{1 + [(f - \nu_o^z)/\gamma_h]^2\} \tag{26}$$

where ν_o^z is a function of n and

$$\alpha_o = 0.182\nu_o(a_1 p/\gamma_h)\theta^3 \exp[a_2(1 - \theta)] \quad \text{dB/km} \tag{27}$$

Additional information has to be provided before the mesospheric O_2 line pattern α_z can be calculated, that is, the polarization of the radio wave and its orientation with respect to the geomagnetic field H. For linearly polarized radiation, an angle of orientation Θ is defined between the wave's magnetic field component in a plane of constant phase (i.e., perpendicular to the direction of propagation) and the geomagnetic field direction H. Line attenuation then generally consists of a mixture of the three Zeeman patterns:

$$\alpha_z = \alpha_1 \cos^2\Theta + (\alpha_2 + \alpha_3) \sin^2\Theta \tag{28}$$

Mesospheric O_2 line properties are direction (anisotropic medium) dependent, as implied by Eq. (28). Further coordinate transformation is necessary when a fixed antenna receives radiation from a mesospheric space element [HARTMANN, 1981].

The patterns $\alpha_{1,2,3}$ of the O_2 lines $K = 1^{\pm}$ to $29^{\pm}$ have been calculated for local p-T-H conditions over the height range 30 to 100 km at two magnetic field strengths, H = 0.3 and 0.6 G. Two examples, $K = 7^{+}$ and 19^{-}, are depicted in Fig. 4. The complete set $K^{\pm} = 1$ to 29 is available upon request (to be published in a report). Above h = 70 km, the individual, now mostly Doppler-broadened components become discernable. Although details depend on specific K values, the relative features at given heights are similar to the cases illustrated in Fig. 4.

The results, in combination with beginning dissociation to atomic oxygen (e.g., at h = 120 km, O_2/O = 0.25), establish h = 100 km as the plausible boundary to outer space for radio path modeling. The cutoff height for water vapor is much lower (h ≈ 20 km).

5. ZENITH PATH ATTENUATION

Cumulative transfer characteristics of the neutral atmosphere are evaluated by a numerical integration of Eq. (21). For a zenith path, the increments dx are equal to dh, and dh is chosen so that each slab is quasi-homogeneous (p, T, e, and w are constant). The formalism developed in Sections 2 to 4 is applied to calculate α(dh) and β(dh). Height profiles of the meteorological quantities are obtained from model atmospheres or in situ data (e.g., radio-sonde). Total precipitable water vapor and hydrometeor absorption, plus the relatively stable dry air attenuation, are the determining quantities of the radio path transfer function (Eq. 22). The water vapor and cloud water column densities(1 g/m^{3}km = 1 mm) are accounted for by

$$V = 7.219 \int_0^{20\ \text{km}} e(h)\theta(h)\, dh \quad \text{mm} \qquad \text{and} \qquad W = \int_0^{10\ \text{km}} w(h)\, dh \quad \text{mm} \tag{29}$$

Dry air attenuation is evaluated for all O_2 lines up to h = 30 km (Sections 2 and 3), and for isolated O_2 lines over the frequency range $\nu_o \pm 100$ MHz by considering the Zeeman effect (Section 4).

A standard example is the one-way zenith response through the U.S. Standard Atmosphere [NOAA, 1976]. Zenith attenuation is displayed in Fig. 5, where the calculation was performed "layer-by-layer", encompassing 58 slabs between h = 0 and 100 km. One notices that outside the O_2 absorption frequency ranges (50 to 70 GHz and 115 to 123 GHz), water vapor V plays the dominant role. The frequency range 53- to 67 GHz is detailed in Fig. 6 assuming conditions (H = 0.3 Gauss, π-pattern) which yield the maximum O_2 line absorption peaks.

A numerical account for selected frequencies in the 45- to 75 GHz range is given in Table II. Maximum shielding ($A_z \geq 150$ dB) of satellite-based systems against interference from ground levels can be achieved between 58.9 and 61.2 GHz. The curve of associated phase dispersion ϕ_z (Eq. 21) is not shown. Frequencies around 57 and 63 GHz yield max/min values of $\phi_m = \pm 14$ radians, while the nondispersive delay of the air mass is

$$t_z(N_0) = 7.64 + 0.21V \quad \text{ns}$$

Both A_z and $|\phi_z|$ increase with decreasing average temperature of the air mass (see x and y, Eq. 23) as is the case for different climates.

As a prospective system operates at increased altitudes, the shielding effect of the unstructured O_2 band shape breaks down and about 30 communication channels open up between the lines (see Fig. 2d, e). The special transfer characteristics of these channels can be evaluated by applying the formulations given in Sections 2 to 4.

Slanted radio paths with elevation angles, $\varphi \geq 6°$ (from horizontal), follow a secant law in clear air, i.e.,

$$A_\varphi = A_z/\sin\varphi \qquad \text{dB} \tag{30}$$

Refinements at low elevation angles consider refractive and dispersive ray bending [HOPPONEN, 1980].

6. PULSE PROPAGATION

Broadband signal transmission at carrier frequencies, f_c = 45 to 75 GHz, through the clear atmosphere has to reckon with the radio path transfer function T_L (Eq. 22). Digital communication systems with high data rates (0.5 to 3 Gbit/s) are possible, employing pulsed signals with durations τ_s in the range 2 to 0.3 ns and requiring transmission bandwidths, BW, between 2 and > 10 GHz. The chances for pulse shape distortion increase when maximum path lengths L are considered, based upon path attenuation A. For example, a terrestrial (h=0 km) system configuration designed to tolerate A = 25 dB could, in principle, operate at 50 GHz over 50 km, which reduces to 1.6 km at 60 GHz.

Calculation of pulse distortion is accomplished as a function of pulse shape, pulse duration, and path length by utilizing, in a mini-computer, the method of Fast Fourier Transform (FFT). The formulation starts with an initial signal waveform

$$e_0(t) = \frac{1}{2\pi}\int_{-\infty}^{\infty} E_0(f)\exp(j2\pi ft)df \tag{31}$$

where e(t) and $E_0(f)$ constitute a voltage signal Fourier transform pair. The signal is assumed to propagate as a plane wave and is received at path length L as

$$e(t,L) = \frac{1}{2\pi}\int_{-\infty}^{\infty} E_0(f)T_L(f)\exp(j2\pi ft)df \tag{32}$$

The nondispersive propagation time (Eqs. 4 and 6)

$$t_L^0 = 3.336(10^6 + N_0)L \qquad \text{ps} \tag{33}$$

is factored out of T_L and numerical evaluations of Eq. (32) are performed with the FFT method [ALLEN and LIEBE, 1982]. Fields of individual spectral components propagate with their own attenuation and velocity, and their superposition at the receiver may lead to considerable pulse shape distortions. Higher frequency components of a pulse signal are sped up with respect to the fundamental for negative gradients of the phase rate $d\beta/df$ and vice versa. The received pulse might experience shortening or lengthening of its original duration; also, it can break up into several parts bearing no resemblance to the original signal, which leads to intolerable bit-error rates.

Propagation properties of sea level air are enumerated in Table III. A more detailed analysis, covering the altitude range h = 0 to 30 km, was reported by LIEBE and HOPPONEN (1977).

Table III. Propagation Properties of Moist Sea Level Air
(0 km, 15°C, 50% RH)

f	GHz	45.0	50.0	53.9	55.8	56.3	60.4	63.0	63.9	65.8	70.0	75.0
α	dB/km	0.18	0.39	2.11	6.37	7.85	15.05	10.70	7.42	2.58	0.59	0.37
β	rad/km	0.22	0.40	0.81	1.01	0.99	-0.17	-1.17	-1.25	-1.03	-0.58	-0.40
$d\alpha/df$	dB/km GHz	0.019	0.093	1.31	3.02	3.10 (+MAX)	0.00	-3.90 (-MAX)	-3.61	-1.46	-0.098	-0.017
$d\beta/df$	rad/km GHz	0.023	0.060	0.15 (+MAX)	0.00	-0.08	-0.41 (-MAX)	-0.22	0.00	0.16 (+MAX)	0.057	0.024

Sea level air presents the most favorable conditions for short-pulse propagation. Frequency gradients of individual O_2 lines at higher altitudes can increase by as much as a factor of 100 on a MHz frequency scale. Examples are given in Fig. 7 for three types of pulse signals operated over a link with the design parameters h = 0 km, clear air, L = 35 km, f_c = 60 GHz, τ_s = 1 ns. The signals considered are:

(a) Gaussian shape requiring minimum BW ($\approx$ 2 GHz).

(b) Rectangular shape requiring maximum BW ($\approx \pm$ 10 GHz).
(c) Binary phase shift key (BPSK) modulation.

Examples of more serious pulse distortions and details of the calculation procedure have been discussed by ALLEN and LIEBE [1982]. It is convenient to include in Eq. (32) the complex frequency response of a BW-limiting device (e.g., receiver bandwidth, smoothing filter, etc.), or a BW-linearizing device (e.g., adaptive phase correction) since average O_2 properties [$\alpha(p,T)$, $\beta(p,T)$] for a given application might be constant.

7. CONCLUSIONS

Moist air has been characterized as an atmospheric propagation medium. The basic physics of molecular absorption in a radio path have been cast into a model with optimum computer run time, but without undue approximations. The paper provides graphical and numerical examples on single frequency and broadband behaviors of typical radio paths operating in the 45 to 75 GHz frequency range. The routines are operated, even by nonexpert users, simply by calling the program name, choosing from a battery of 10 model atmospheres, and typing in the interactively requested input parameters -- meteorological data are converted into propagation data.

The program is available in FORTRAN IV upon request, together with print-outs at selected frequencies [f = 45, 46, 47,... GHz; $f = \nu_0$; and $f = (\nu_0' + \nu_0'')/2$] over 48 height levels h = 0 to 30 km for a model atmosphere (arctic-to-tropical). Displayed are values of α, $d\alpha/df$, β, $d\beta/df$, A_z, B_z, V, W, and t_z^o for relative humidities, RH = 0 to 100%, specified over h=0 to 8 km. Cloud and statistical rain attenuation models are also available. Shortcomings of the present model lie in the omitted spectroscopic data base for trace gases and in the empirical nature of the water vapor contribution to Eq. (16).

Detrimental effects such as fluctuations in amplitude [MEDEIROS-FILHO et al., 1981], phase, and group velocities, and the direction of the radio wave, may be predicted from spatial and temporal variations of p-T-e-w distributions along a radio path. A priori assessments can be made of rare events for reliable system operations and of possible bandwidth limitations.

ACKNOWLEDGMENTS

The author wishes to thank K. C. ALLEN, who performed the pulse shape calculations depicted in Fig. 7 and contributed valuable comments. The work was partially supported by the U.S. Army Research Office under contract ARO 6-82.

8. REFERENCES

ALLEN, K. C. and H. J. LIEBE, 1982, "Pulse distortion in atmospheric EHF propagation," to be published.

BROWN, D. R., 1982, "Dispersion profiles for near millimeter wave refractivity," to be published.

HARTMANN, G. K., 1981, "The Zeeman-effect of O_2 and its application to the investigation of the Earth's atmosphere," Technical Report MPAE-W-66-81-22, Max-Planck-Institut Aeronomie, Fed. Rep. Germany, October, 32 pp.

HOPPONEN, J. D., 1980, "Simulation of EHF propagation through the atmosphere," AGARD-CP-284, 6/1-11.

LIEBE, H. J., 1981, "Modeling attenuation and phase of radio waves in air at frequencies below 1000 GHz," Radio Sci. 16(6), 1183-1199.

LIEBE, H. J. and J. D. Hopponen, 1977, "Variability of EHF air refractivity with respect to temperature, pressure, and frequency," IEEE Trans. Ant. & Prop. AP-25(3), 336-345.

LIEBE, H. J., G. G. GIMMESTAD, and J. D. HOPPONEN, 1977, "Atmospheric oxygen spectrum - experiment vs. theory," IEEE Trans. Ant. & Prop. AP-25(3), 327-335.

MEDEIROS-FILHO, F. C., D. A. JAYASURIYA, and R. S. COLE, 1981, "Spectral density of amplitude scintillations on a 55 GHz line of sight link," Electron. Letters 17(11), 24-25.

NOAA, 1976, "U.S. Standard Atmosphere, 1976, "Monograph NOAA-S/T 76-1562, U.S. Government Printing Office, Washington, D.C.

ROSENKRANZ, P. W., 1975, "Shape of the 5 mm oxygen band in the atmosphere," IEEE Trans. Ant. & Prop. AP-23, 498-506.

Table I. Selected Specific Attenuation (α) and Phase (β) Rates at Altitudes h=0 to 30 km for U.S. Std. Atm. [NOAA, 1976].

h	RH	f, GHz	60.306	60.400	60.435	60.800	61.151	61.500	61.800	62.100
		ν_o	5-		7+		9+		11+	
km	%					dB/km rad/km				
0	50	α	15.1	15.1	15.1	15.1	14.9	14.6	14.1	13.6
		β	- 0.119	- 0.145	- 0.172	- 0.318	- 0.464	- 0.599	- 0.736	- 0.864
2	50	α	13.7	13.8	13.8	13.6	13.3	13.1	12.7	12.1
		β	- 0.126	- 0.152	- 0.179	- 0.321	- 0.454	- 0.574	- 0.699	- 0.821
6	50	α	11.3	11.3	11.3	10.7	10.3	9.93	9.72	9.39
		β	- 0.124	- 0.157	- 0.191	- 0.329	- 0.420	- 0.497	- 0.583	- 0.683
10	50	α	9.51	9.58	9.48	7.74	7.60	6.83	7.05	6.74
		β	- 0.085	- 0.145	- 0.212	- 0.339	- 0.372	- 0.409	- 0.444	- 0.499
15	2	α	6.56	6.93	6.70	2.86	4.63	2.51	4.14	2.67
		β	0.067	- 0.067	- 0.213	- 0.222	- 0.200	- 0.213	- 0.207	- 0.203
20	2	α	4.52	4.79	4.89	0.71	3.71	0.63	3.23	0.69
		β	0.140	- 0.011	- 0.196	- 0.112	- 0.093	- 0.100	- 0.092	- 0.080
25	1	α	3.20	1.65	3.78	0.14	3.39	0.10	2.94	0.21
		β	0.083	0.006	- 0.105	- 0.043	- 0.034	- 0.036	- 0.033	- 0.039
30	0	α	2.91	0.57	3.38	0.03	3.28	0.03	2.86	0.03
		β	0.047	0.004	- 0.056	- 0.022	- 0.017	- 0.019	- 0.017	- 0.014

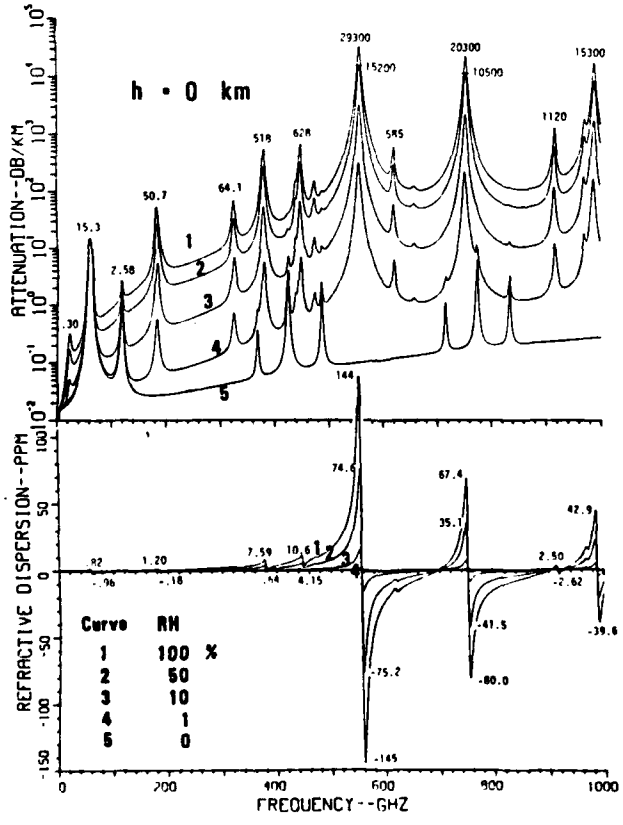

Figure 1. Attenuation α in decibels per kilometer and refractive dispersion D in parts per million for dry (RH = 0%) to saturated (RH = 100%) air at sea level (h = 0 km) for the U.S. Standard Atmosphere [NOAA, 1976] over the frequency range f = 1 to 1000 GHz [LIEBE, 1981].

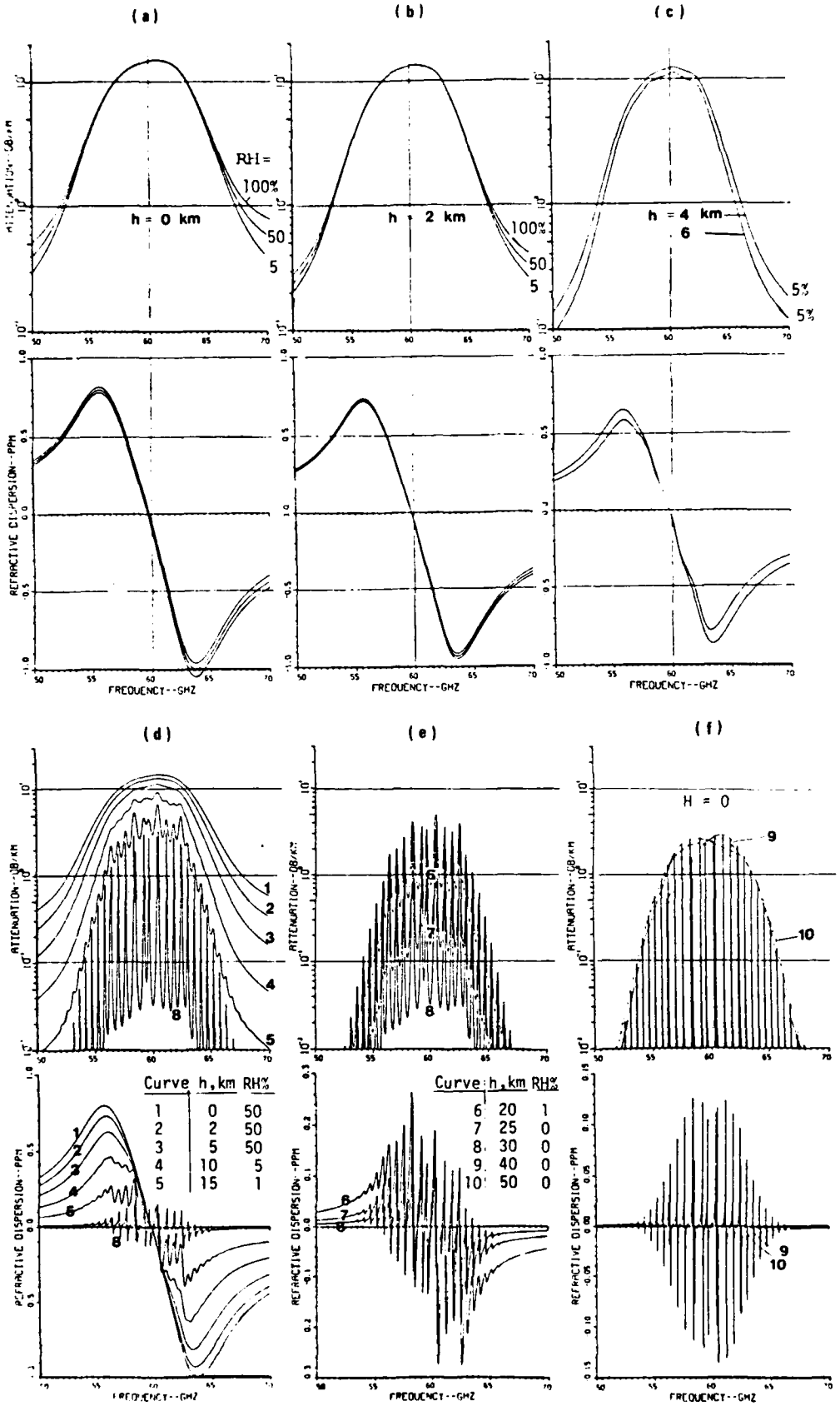

Figure 2. Attenuation α in decibels per kilometer and refractive dispersion D in parts per million of air (U.S. Std. Atm.) at various altitudes h and relative humidities RH, (a) to(f), over the frequency range f = 50 to 70 GHz.

Table II. Evaluation of Zenith Attenuation A for U.S. Std. Atm. 76 (Water Vapor V=15 mm) Between 45- and 75 GHz, Including Mesospheric Zeeman Effects

f	$f = \nu_0$	α (Figs. 2,3) h=0	α (Figs. 2,3) 30 km	A (Fig. 5) h=0 to 30 km	$A_1(0.3)$ (Fig. 4) h=30 to 100 km	$A_1(0.6)$ (Fig. 4) h=30 to 100 km	A_z (Fig. 6) h=0 to 100 km
GHz	K±	dB/km		dB	dB		dB
45.00		.18	.00	.68			.8(1)*
50.00		.39	.00	1.64			1.7(1)
52.00		.76	.00	3.33			3.5(2)
54.00		2.30	.00	12.6			12.6(3)
55.22	19-	4.77	.45	38.9	17.8	15.1	55 (1)
57.61	11-	11.6	2.46	146	83.3	71.8	224 (6)
57.97		12.3	.02	119			120 (1)
58.32	9-	13.0	2.99	190	97.7	84.5	281 (7)
58.45	3+	13.2	1.94	180	68.1	61.0	245 (3)
58.81		13.8	.03	139			140 (1)
59.16	7-	14.2	3.11	195	102	89.1	291 (6)
59.95		14.4	.03	159			160 (1)
60.31	5-	15.1	2.91	223	92.8	81.6	310 (6)
60.43	7+	15.1	3.38	228	114	99.1	335 (7)
60.79		15.1	.03	151			151 (1)
60.15	9+	14.9	3.28	196	113	98.2	302 (8)
61.48		14.6	.03	139			139 (1)
61.80	11+	14.2	2.86	180	100	86.9	274 (7)
62.11		13.6	.03	134			134 (1)
62.41	13+	12.8	2.42	179	80.2	69.2	254 (5)
62.49	3-	12.5	2.18	171	69.2	62.3	237 (4)
62.74		11.7	.03	113			113 (1)
63.00	15+	10.7	1.59	117	59.1	50.4	172 (5)
65.77	25+	2.58	.08	13.9	3.73	3.18	17.7(4)
66.00		2.26	.00	10.7			10.8(2)
68.00		.94	.00	3.83			4.0(2)
70.00		.59	.00	2.27			2.5(2)
75.00		.37	.00	1.22			1.4(2)

*Number in parenthesis indicates variability of the last digit shown due to humidity and magnetic field strength.

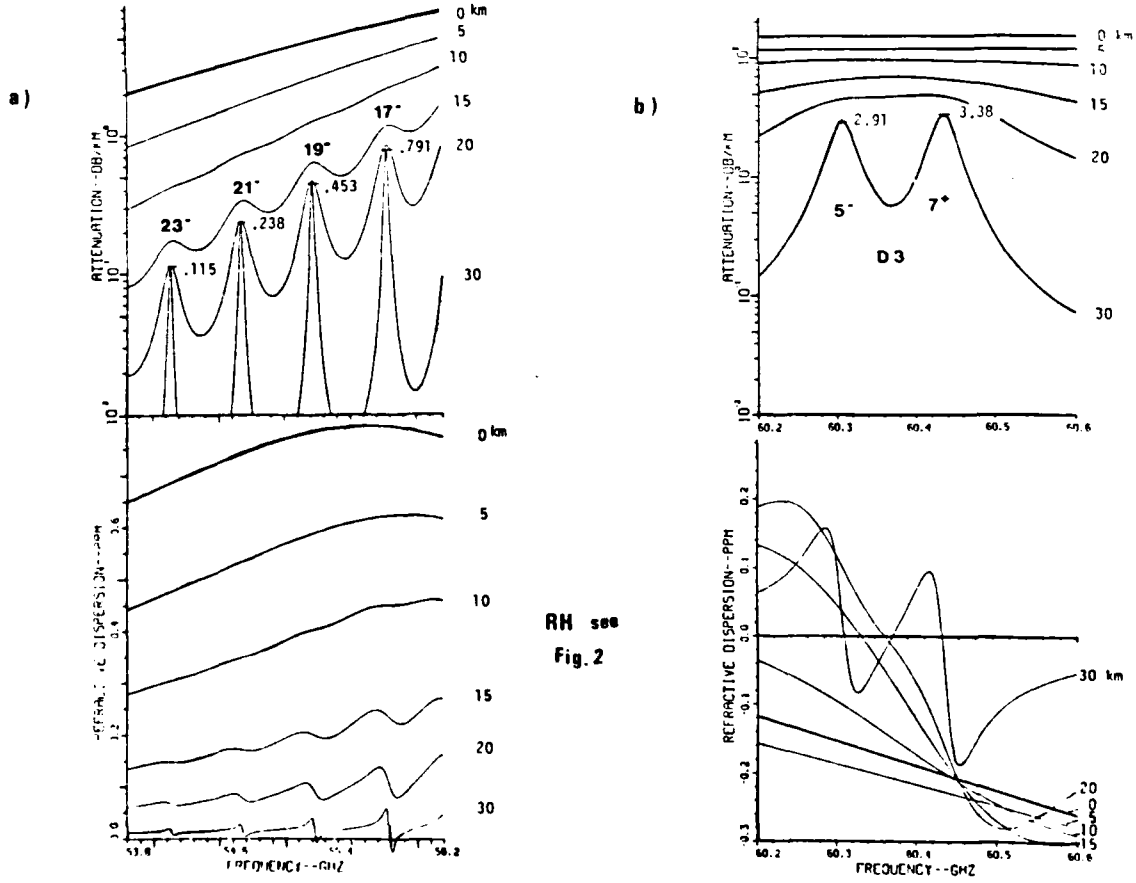

Figure 3. Attenuation α in decibels per kilometer and refractive dispersion D in parts per million in the oxygen microwave band at altitudes h = 0-30 km (U.S. Std. Atm.).

a) f = 53.8 to 56.2 GHz, b) f = 60.2 to 60.6 GHz.

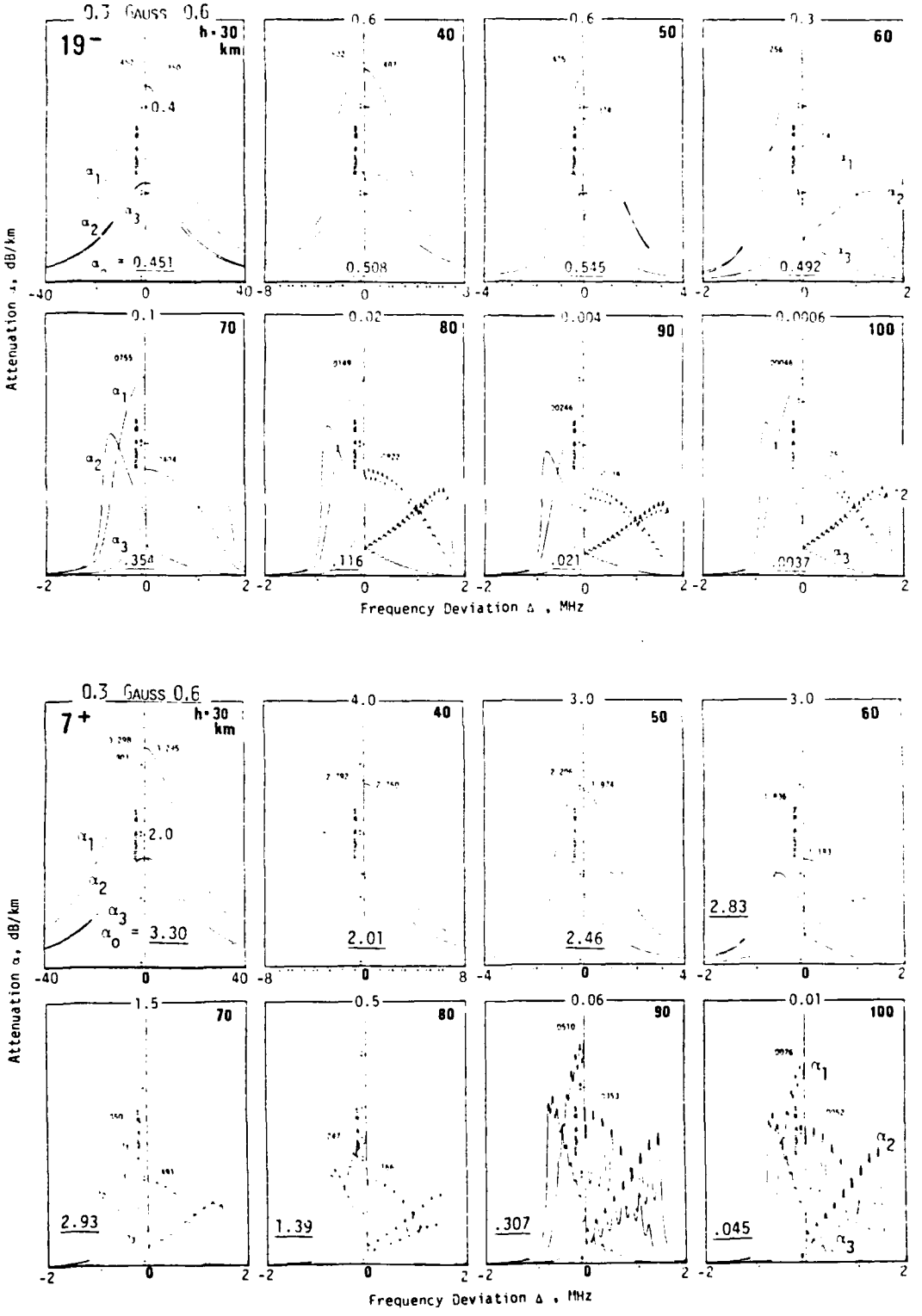

Figure 4. Zeeman attenuation patterns of the oxygen microwave lines K = 19^- (see Fig. 3a) and 7^+ (see Fig. 3b) for altitudes h = 30-100 km (U.S. Std. Atm.). Each frame displays $\pi(\alpha_1)$, $\sigma^+(\alpha_2)$, and $\sigma^-(\alpha_3)$ patterns for the magnetic field strengths H = 0.3 (left hand) and H = 0.6 G (right hand). The patterns are symmetric with respect to the center axis (interchange σ^+ and σ^-). The frequency deviation $\Delta = (f - \nu_0)$ is between ±40 MHz for h = 30 and ±2 MHz for h = 60-100 km. The maximum attenuation rate α_0 is that of the isolated unsplit line (H = 0 and $f = \nu_0$).

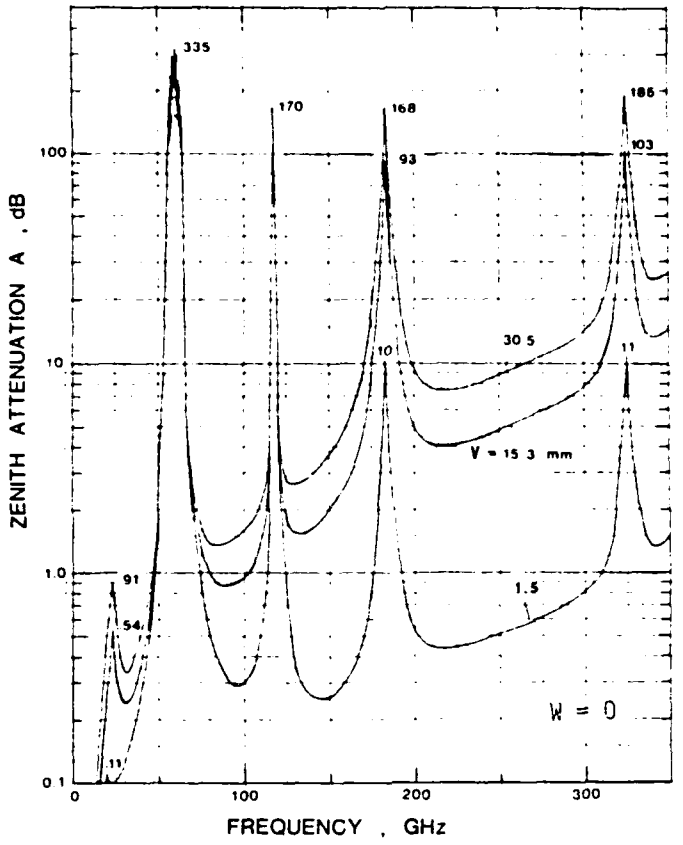

Figure 5. Zenith attenuation A in decibels of the U.S. Std. Atm. for a cloud-free, dry (V = 1.5 mm), moist (15.3 mm), and saturated (30.5 mm, RH = 100% for h = 0 to 8 km) air mass over the frequency range f = 10 to 350 GHz.

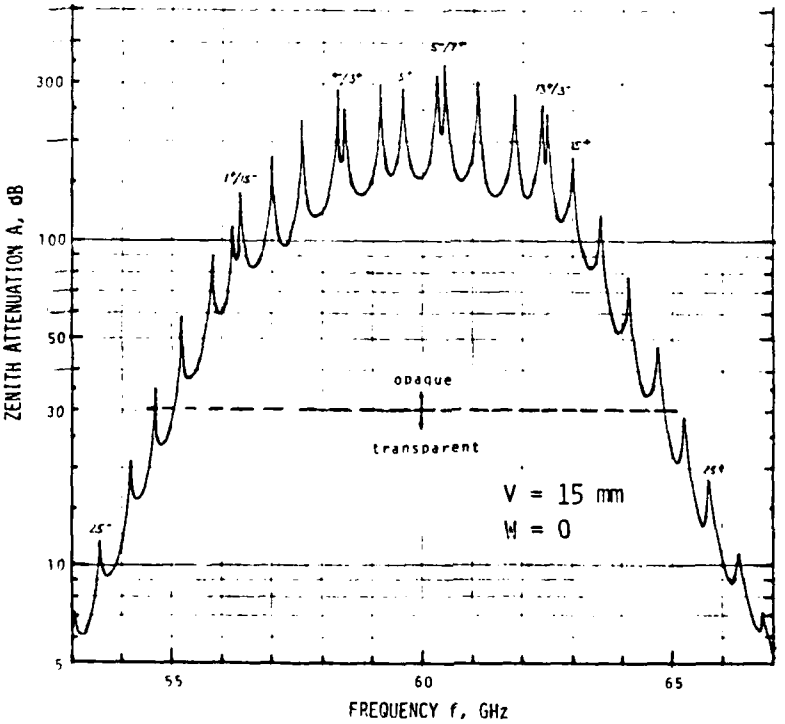

Figure 6. Details of zenith attenuation A (V = 15 mm, see Fig. 5) over the frequency range f = 53 to 67 GHz exhibiting 60 GHz oxygen absorption with band and complete line structure. A π-type Zeeman pattern (α_1) (see Fig. 4) and H = 0.3 Gauss were assumed for the height range h = 30 to 100 km.

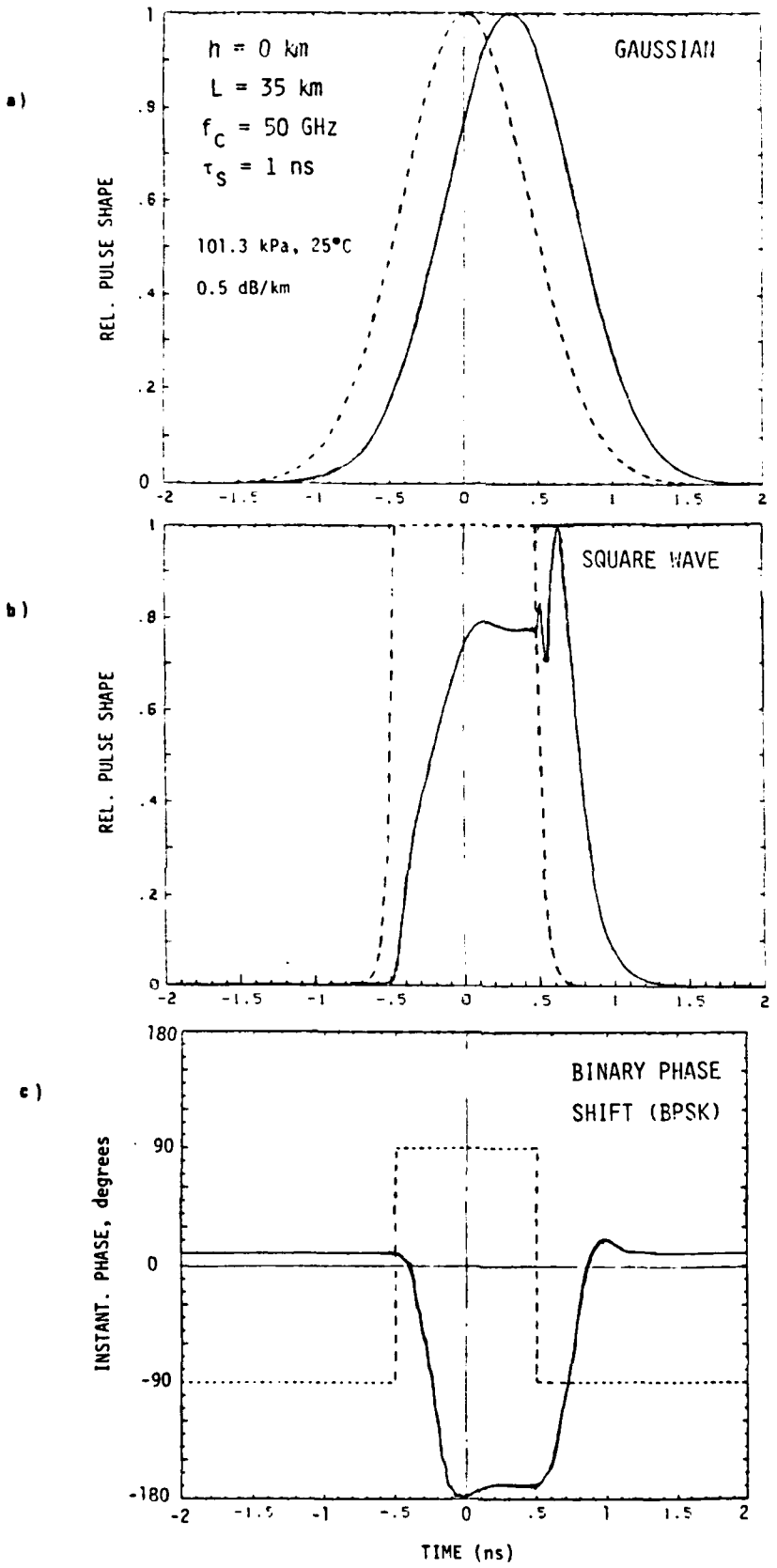

Figure 7. Relative pulse shape distortion over a terrestrial path of 35 km length at the carrier frequency of 50 GHz using Gaussian, rectangular, and BPSK 1-ns-wide test signals (dashed line).